Comprehensive Radiation and Imaging Isocenter Verification Using NIPAM kV-CBCT Dosimetry

by

Kiran Elizabeth Pant

Department of Medical Physics
Duke University

Date:_____

Approved:

_____
Justus Adamson, Advisor

_____
William Giles

_____
Mark Oldham

_____
Scott Floyd

Thesis submitted in partial fulfillment of
the requirements for the degree of Master of Science in the Department of
Medical Physics in the Graduate School
of Duke University

2020

ABSTRACT

Comprehensive Radiation and Imaging Isocenter Verification Using NIPAM kV-CBCT Dosimetry

by

Kiran Elizabeth Pant

Department of Medical Physics
Duke University

Date:_____

Approved:

_____
Justus Adamson, Advisor

_____
William Giles

_____
Mark Oldham

_____
Scott Floyd

An abstract of a thesis submitted in partial fulfillment of the requirements for the degree of Master of Science in the Department of Chemistry in the Graduate School of Duke University

2020

Abstract

Purpose: To develop a comprehensive method to measure the radiation uncertainty and coincidence with the kV-CBCT imaging coordinate system using NIPAM kV-CBCT dosimetry.

Methods: An N-isopropylacrylamide (NIPAM) dosimeter is irradiated at eight gantry/couch combinations which enter the dosimeter at unique orientations such that the beams do not overlap except at the isocenter. 1-3 CBCT images are acquired before and immediately after irradiation, radiation profile is detected per beam, and the displacement from the imaging isocenter is quantified. This test has been performed on SRS cone sizes ranging from 4 mm to 15 mm diameter and a 5 mm diameter MLC field, delivering approximately 16 Gy per beam. Matlab code was developed in house to detect each beam's geometry and to quantify relevant parameters, including radiation isocenter and coincidence with the CBCT origin and the actual gantry and couch angles per beam. The dose profile of each beam was detected in the CBCT using the contrast-to-noise ratio (CNR) of the irradiated high dose regions relative to the surrounding background signal of the dosimeter. Reproducibility was demonstrated by repeating the test on two separate NIPAM dosimeters using the 6 mm cone. To determine the robustness of our test, our results were compared to the results of the traditional Winston-Lutz test, film based "star shots," and the Varian Machine Performance Check

(MPC). The ability of our Matlab code to detect alignment errors was demonstrated by applying a 0.5 mm shift to the MLCs in the direction of leaf travel.

Results: Setup, irradiation, and imaging can be completed in under 40 minutes. The minimum radius to encompass all beams calculated by automated analysis for the MLCs, 4 mm cone, 6 mm cone, 7.5 mm cone, 12.5 mm cone, and 15 mm cone was 0.38 mm, 0.44 mm, 0.53 mm, 0.48 mm, 0.75 mm, 0.5 mm, and 0.57 mm, respectively. When determined manually, these values slightly decreased to 0.28 mm, 0.40 mm, 0.33 mm, 0.41 mm, 0.61 mm, 0.48, and 0.34 mm, respectively. The isocenter verification test was repeated using the 6 mm cone; in both tests, the smallest radius to encompass all beams was found to be 0.53 mm, indicating that the test is reproducible. For comparison, the 3D isocenter radius was 0.24 mm, 0.25 mm, and 0.28 mm for the traditional Winston-Lutz test with MLCs, the Varian MPC, and a "star shot" QA sample. Lastly, when a 0.5 mm shift was applied to the MLCs, the smallest radius to encompass all beams increased from 0.38 mm to 0.90 mm.

Conclusion: The results of this project demonstrate the feasibility of a comprehensive isocenter verification test using NIPAM kV-CBCT dosimetry which incorporates the evaluation of radiation coincidence with the imaging coordinate system, and is capable of producing sub-mm results. This test is applicable to all SRS cone sizes as well as MLCs and can be performed in a typical QA time slot.

Contents

List of Tables

List of Figures

Acknowledgements

I have many thanks to give, but I owe most of them to my advisor, Dr. Justus Adamson. Without his constant support, guidance, and dedication I would not have accomplished all that I did in my time at Duke University. I would also like to thank the other members of my thesis committee, Dr. Mark Oldham, Dr. Will Giles, and Dr. Scott Floyd, for their insightful feedback and suggestions on my research. This work would not have been possible without them.

To the Duke Medical Physics Graduate Program, thank you for giving me the tools necessary to succeed as a student and researcher. To my classmates, thank you for encouraging me to become the best version of myself. Sabrina, thank you for deriving the equation used to determine the number of Grey's Anatomy episodes we would watch per day. I could not have done this without you.

Lastly, to my parents. Thank you for your constant support and for always believing in me. To the women in the field of medical physics, never stop believing.

1. Introduction

1.1 Clinical background

New diagnoses and therapy techniques are substantially improving the cancer survival rate in the United States[1]. In particular, stereotactic body radiation therapy (SBRT) of various cancers and stereotactic radiosurgery (SRS) of brain cancer and metastases have shown to be highly effective in both palliative and curative therapy for patients[2–4]. Both SBRT and SRS irradiate lesions with high doses in a small number of fractions, as compared to conventional radiotherapy which will deliver less dose in more fractions. Over the past decade, much research has been conducted in the areas of imaging and dosimetry to improve upon the current standards of SBRT and SRS to ensure radiation dose is limited to adjacent healthy tissues.

Advances in imaging have significantly improved the clinical workflow of treating patients with SBRT/SRS. Today, most linear accelerators are equipped with a kilovoltage imaging system that is capable of acquiring cone-beam computed tomography (kV-CBCT, or CBCT) images[5]. This is especially beneficial during SBRT/SRS treatment as the kV-CBCT imaging system may be used for the verification of patient alignment[6] and the evaluation of organ motion before and after treatment[7]. It has also allowed for sufficiently small margins to be used in SBRT, often making dose escalation possible[8,9], and is heavily used in SRS for accurate patient setup[10]. Historically, patients were aligned using external stereotactic frame systems which required fixing the unit to

the patient's skull. On-board kV-CBCT is increasingly replacing this uncomfortable procedure by aligning a frameless mask using the imaging system[11].

The spatial accuracy of the radiation and kV-CBCT systems is of the utmost importance, especially given the role in which the imaging system is used for SBRT/SRS[12]. Per TG-142, the spatial accuracy of the linear accelerator radiation system must be tested and verified at regular intervals depending on the utilization of the machine[13,14]. Many different quality assurance (QA) tests are used to verify spatial accuracy, including "star shots"[15] and the Winston-Lutz test[16], as well as vendor-provided tests such as the Varian Machine Performance Check (MPC)[17]. However, the majority of these QA tests do not evaluate the coincidence of the radiation isocenter with the imaging coordinate system; this is typically accomplished through separate QA tests[18].

As radiation therapy treatment becomes more complex, the need for more accurate QA tests increases. High-resolution three-dimensional (3D) dosimetry systems may offer more comprehensive QA tests and provide a unique methodology for measuring dose distributions achieved by techniques such as SBRT/SRS[19]. In particular, 3D polymer gel dosimetry research has exploded over the last decade for its specific advantages over one- and two-dimensional systems in a clinical setting. However, many clinics are not implementing protocols using 3D dosimetry due to lack of specialized equipment needed for readout, and the additional workload requirements needed for

analysis. In this study, we present a novel technique for isocenter verification using a 3D gel dosimeter which may be read out using the kV-CBCT imaging system.

1.2 Three-dimensional (3D) dosimetry

Current 3D dosimetry systems include plastic radiochromic leuco-dye dosimeters (PRESAGE)[20], normoxic polyacryladmide gels PAGAT[21], and N-isopropylacrylamide (NIPAM)[22] dosimeters. Specifically, PRESAGE has been investigated thoroughly for over a decade to determine its potential as a 3D dosimeter. The robustness, reproducibility, and accuracy of the radiochromic response of the dosimeter supports its claim to be a viable 3D dosimetry tool[23], while also showing to have favorable characteristics for optical CT dose readout[24]. Similarly, PAGAT dosimeters are a viable 3D dosimetry tool when coupled with magnetic resonance imaging[21]. Although these imaging modalities can accurately and effectively read out the dose distributions of the respective dosimeters, they are not always readily available in a standard clinic. This presents the major challenge of using 3D dosimetry: widespread use is prohibited due to lack of necessary equipment.

In comparison, NIPAM dosimeters can be read out on the on-board kV-CBCT imaging system. These dosimeters are fabricated from radiation sensitive materials that polymerize as a function of absorbed dose upon irradiation[25], leading to a change in density. Dose visualization is possible due to this change within the gel dosimeter[26], which results in a change in intensity (i.e. Hounsfield unit)[25] in the kV-CBCT image.

Because the imaging system is incorporated in the linear accelerator radiation system, the read out will be in the same frame of reference as the radiation delivered.

The idea to use polymer gel for radiation therapy purposes was first introduced in 1950 by Day and Stein, who showed that radiation produced color changes to gels containing dye[27]. Many different formulations have since been developed, with an emphasis on increasing dose sensitivity and reducing chemical toxicity of the gels. Specifically, NIPAM has been shown to have reduced toxicity compared to other monomers[28], while also increasing x-ray CT sensitivity[26,29].

1.3 Motivation of current study

The purpose of this study is to demonstrate a comprehensive isocenter verification technique in which the radiation isocenter is imaged and quantified using NIPAM kV-CBCT dosimetry. Prior work[29] focused on demonstrating proof of principle of visualizing the delivered dose directly; the focus of this study is to utilize this technology to develop a technique to measure and quantify the spatial uncertainty of the radiation isocenter and its coincidence with the kV-CBCT imaging system.

2. N-isopropylacrylamide (NIPAM) dosimeters

2.1 NIPAM dosimeter preparation and storage

NIPAM dosimeters were prepared at Duke University's 3D Dosimetry and Optical Bio-Imaging Laboratory under a fume hood. Each step of the procedure was carefully controlled, including the timing and temperature at each step of the fabrication process to ensure reproducibility of each gel dosimeter. Table 1 shows the list of ingredients (as a percentage of weight) used in each dosimeter.

Table 1: Composition of NIPAM dosimeters used in this study.

Component	*Relative Composition*
Deionized water	75.5%
Gelatin (Sigma-Aldrich, Oakville, ON, Canada)	5%
N-isopropylacrylamide (TCI America, Portland, OR, USA)	15%
N,N'-methylenebisacrylamide (Sigma-Aldrich)	4.5%
Tetrakis Hydroxymethyl Phosphonium Chloride (Sigma-Aldrich)	5 mM

To begin the fabrication process, gelatin and deionized water were mixed and brought to a temperature of 40 ± 0.5° C. Once the gelatin had completely dissolved, NIPAM was added and the mixture's temperature was reduced to 34 ± 0.5° C. After

allowing the NIPAM to dissolve, N-N'-methylenebisacrylamide (BIS) was added and the mixture's temperature was cooled to 30 ± 0.5° C. Then, tetrakis hydroxymethyl phosphonium chloride (THPC) was added to the mixture using a pipette and stirred for exactly one minute and fifteen seconds.

The gel was then poured into a 1-L (16 oz.) cylindrical jar made of Polyethylene Terephthalate (PET) plastic with a 7.5 cm diameter and 13.1 cm height. In order to minimize oxygen effects, mineral oil was added to the top of the liquid to displace air above the gel. The top was then covered in parafilm prior to capping, and the PET jars were vacuum-sealed in food storage packaging to further prevent oxygen effects. The dosimeters were placed in the refrigerator (4° C) and allowed to set for 6-8 hours. A prepared dosimeter is shown in Figure 1.

Figure 1: Fabricated NIPAM dosimeter prepared in Duke University's 3D Polymer Gel Dosimetry and Optical Bio-Imaging Lab.

Total fabrication time for one dosimeter is approximately one hour. On average, the dosimeters were stored in the refrigerator for 4 days prior to being removed for imaging and irradiation.

2.2 Cost analysis

One question that arises with using the NIPAM dosimeters is whether the cost of production is prohibitive for routine QA. Table 2 shows the cost breakdown analysis to fabricate a 16 oz. dosimeter.

Table 2: Cost analysis of a 16 oz. NIPAM dosimeter.

Ingredient	*Bulk Quantity*	*Bulk Cost*	*Quantity used in 16 oz. PET jar*	*Cost/jar*
Water	3,785.41 mL	$25.00	350 mL	$2.31
Gelatin	1,000 g	$155.00	22.5 g	$3.49
NIPAM	500 g	$226.00	67.5 g	$30.51
BIS	500 g	$110.00	20.25 g	$4.46
THPC	500,000 μL	$184.00	400 μL	$0.15
16 oz. PET jar	24	$27.36	1	$1.14

Thus, the cost of producing one 16 oz. NIPAM dosimeter is roughly $40. This is likely feasible for less frequent routine QA, such as annual QA, after maintenance of a

machine, or perhaps monthly QA; but is likely less feasible for more frequent QA such as replacing daily Winston Lutz QA. While we fabricate the dosimeters in house, it would be expected that these could be purchased from a commercial manufacturer in the case of routine clinical use. It is likely that the cost of one 16 oz. dosimeter would decrease slightly by purchasing directly from the manufacturers.

3. Preliminary measurements using NIPAM dosimeters

3.1 Introduction

Before implementing our comprehensive isocenter verification test using NIPAM kV-CBCT dosimetry, we first perform several experimental measurements to develop and optimize our test. Specifically, we are interested in determining (1) the optimal CBCT acquisition parameters to maximize the signal of the NIPAM dosimeter in the CBCT image, and (2) the sensitivity of the dosimeters over time to investigate the signal response in varying timeframes between irradiation and imaging, as well as to determine to longevity of the dosimeters when stored both at room temperature and in the refrigerator.

3.2 CBCT acquisition parameters

3.2.1 Overview

The purpose of this experiment is to determine the optimal CBCT acquisition parameters for imaging the NIPAM dosimeters. We want to minimize the amount of noise in the CBCT without saturating the image or overheating the kV tube during image acquisition. Previous work[29] focused on utilizing image processing to improve the visibility of the dose distribution in the CBCT, whereas we are focused on investigating CBCT acquisition parameters to improve visibility.

3.2.1 Materials and methods

To determine the optimal CBCT parameters, a NIPAM dosimeter was placed on the treatment couch and irradiated using a 4x4 cm field size using opposed fields (90° and 270°), which are delivered within 3 minutes of each other, and 1066 monitor units (MU) per beam, totaling approximately 20 Gy per beam. The dosimeter was removed from the table and allowed to sit for one hour to stabilize the effect of increasing CNR over time due to the chemical polymerization process of the dosimeter. After one hour, on-board CBCT images were acquired of the dosimeter to determine the acquisition parameters that resulted in a maximum CNR value without saturating the image or overheating the kV tube. The image sets were acquired at 80, 100, and 125 kVp using full fan scan and full arc trajectory. The mAs value was set to the maximum setting that did not result in saturation of the projected images. For each CBCT, raw CNR was obtained using region of interests (ROIs) (roughly 2 cm squares) in the irradiated field and un-irradiated fields of the dosimeter, and was calculated as the difference between the mean signal in the irradiated and un-irradiated ROIs, divided by the standard deviation of the signal in the un-irradiated ROI.

A slow-mode CBCT setting was also explored. It was found that using a slower setting increased the number of projections from 895 to 5,330. Similar to the previous experiment, different mAs settings were applied to an irradiated dosimeter at 125 kVp.

Because of the length of the scan, the primary concern in determining the optimal mAs setting was overheating the kV tube during image acquisition.

There are also various reconstruction filter options (smooth, standard, sharp, and ultrasharp) on the on-board kV-CBCT system (Varian STx). To quantify the tradeoff between CNR and spatial resolution, we used a CTP528 high resolution module of a Catphan 504 phantom. The phantom was set up according to the manufacturer's instructions[30], a CBCT image was acquired (full fan scan with full trajectory, 125 kVp, 1030 mAs, smooth reconstruction, and 1 mm slice thickness), and the image was reconstructed using the four different reconstruction filters. The DICOM files were exported and loaded into Spyder (version 3.3.6), and the Pylinac package was utilized to analyze the high-contrast line pairs from the CTP528 module to calculate the modulation transfer function (MTF). The MTF is often used as a metric to incorporate both spatial resolution and noise (contrast) into a single specification.

3.2.2 Results

Table 3 summarizes the results of determining the optimal CBCT acquisition parameters that resulted in no saturation of the image or overheating of the kV tube using a standard scan.

Table 3: Experimental measurements investigating CBCT acquisition parameters for NIPAM dosimeters.

kVp	*Optimal mAs*	*CNR*
80	5337.5	5.9

100	2137.5	4.3
125	1080	6.9

The mAs values were the result of the of the kV tube not overheating in a single scan, thus the panel saturation was the limiting value in maximizing the mAs setting. We found that the optimal CNR was achieved for a full arc CBCT imaged at 125 kVp with 1080 mAs.

For the slow-mode CBCT, we found that the optimal acquisition parameters for a full arc CBCT were 125 kVp with 5130 mAs. The scan takes six minutes to complete, and, on average, raises both the anode and housing units in the kV tube by approximately 45%.

When reconstructed with the smooth, standard, sharp, and ultrasharp reconstruction filters the CNR of the dosimeter was 2.85, 2.55, 2.13, and 1.68, respectively. Thus, the smooth reconstruction filter provided the highest CNR value. One concern of using the smooth reconstruction filter is the potential loss of spatial resolution. The MTF 50% (line pairs/mm), as determined by the Pylinac package, for the CTP528 high resolution module using smooth, standard, sharp, and ultrasharp reconstruction filters was 0.75, 0.88, 1.01, and 1.14, respectively. Figure 2 shows the MTF curves for each reconstruction method. As shown in Figure 2, most of the degradation in spatial resolution for the smooth reconstruction filter occurs above the Nyquist limit

for 1 mm dose resolution grid, which justifies our decision to apply the smooth reconstruction filter to the CBCT image of the NIPAM dosimeter.

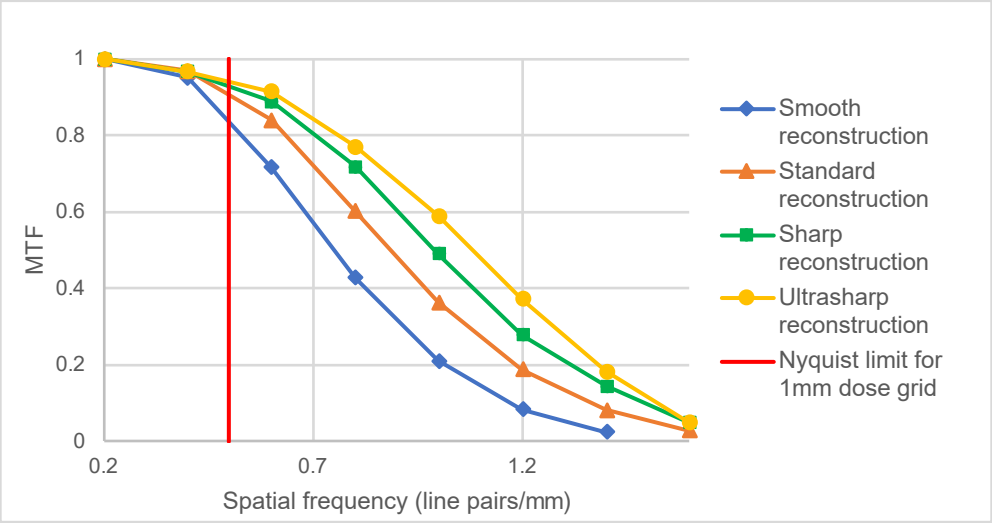

Figure 2: MTF curves for the smooth, standard, sharp, and ultrasharp reconstruction filters.

3.3 Dosimeter sensitivity over time

3.3.1 Overview

Traditionally, NIPAM dosimeters are read out on diagnostic CT systems after 24 hours to allow the chemical reactions and dose sensitivity to stabilize[31]. However, imaging the dosimeter in a much quicker timeframe is desirable for the purpose of our novel isocenter verification test for the practicality reason of being able to use the dosimeter during a typical QA session. Also, by not moving the dosimeter in between irradiation and imaging, we ensure the radiation dose is inherently aligned with the imaging coordinate system, an important advantage of our test. Because of this, we investigated the changes in the dosimeter signal over a time span of 30 to 60 minutes.

We are also interested in quantifying the longevity (shelf life) of the NIPAM dosimeters, both when left at room temperature and in the refrigerator. Because the purpose of these dosimeters is to use them during a QA session, it would be logistically easier to store the dosimeters on-site or purchase them ready-made and delivered, rather than fabricating them immediately prior to use. By evaluating the shelf life of NIPAM dosimeters, we can determine the optimal usage time from the moment of fabrication (or delivery) to irradiation and imaging.

3.2.2 Materials and methods

Eight NIPAM dosimeters were fabricated in 8 oz. PET jars (5.8 cm diameter, 10.9 cm height) and placed in a refrigerator to set. To evaluate the sensitivity over time, a pre-irradiation CT image was acquired of the dosimeter on a GEHC Discovery CT590 RT using 80 kVp and 440 mAs. The dosimeter was then irradiated using opposed fields (4x4 cm fields at 90° and 270°, delivering approximately 20 Gy total). After the irradiation, the dosimeter was returned to the GEHC Discovery CT590 RT and a post-irradiation CT image was acquired, and the contrast between the pre- and post-irradiation Hounsfield Units (HU) was determined. A follow-up diagnostic CT image was acquired every 15 minutes for up to 120 minutes, and the CNR between the pre- and post-irradiated HU in a ROI (roughly 1 cm squares) was calculated for each follow-up image.

To evaluate the longevity (shelf life) of the NIPAM dosimeters, half of the eight dosimeters were stored in a refrigerator while the other half remained at room temperature. Both sets of the dosimeters were irradiated and imaged at 1, 3, 5, 11, 22, and 30 days post fabrication. Experiments were performed in two separate batches; after the first batch of dosimeters were used (imaged at 1, 3, 5, and 30 days post-fabrication), it was found that more data points be beneficial between days 5 and 30, and thus and the next batch was imaged and irradiated at 11 and 22 days post-fabrication. On the day of irradiation, a pre-irradiation diagnostic CT image was acquired, the dosimeter was irradiated, and a follow-up CT image was acquired. The contrast was then calculated as the difference between the HU inside and outside the irradiated region of the dosimeter.

3.2.3 Results

Figure 3 shows the CNR over time for the dosimeters used in this experiment. For the refrigerated dosimeter irradiated 5 days post-fabrication, the CNR increased by 60%, 86%, and 102% after waiting 15 minutes, 30 minutes, and 60 minutes after irradiation, reaching a peak of 6.8 after 75 minutes. By waiting 24 hours after irradiation, the CNR of the room temperature and refrigerated dosimeter irradiated one day post-fabrication increased by 120% and 154% from the first time point, respectively.

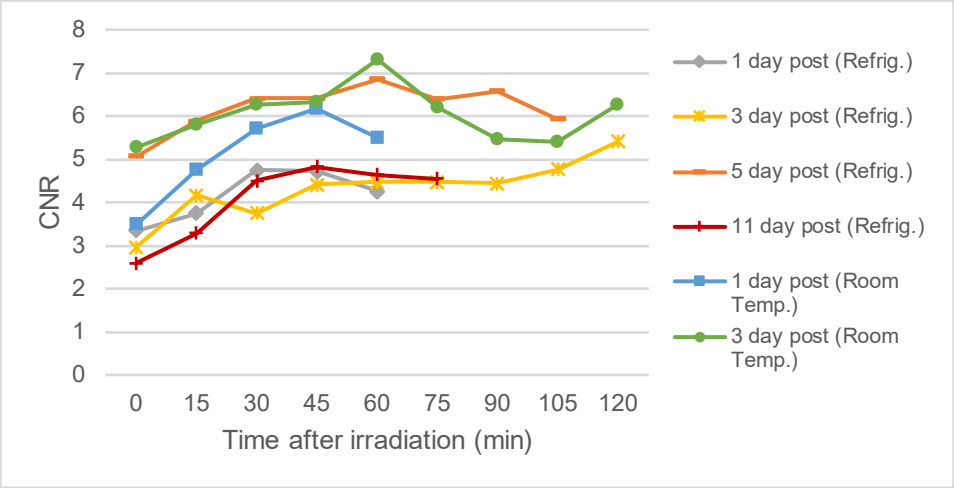

Figure 3: CNR versus time after irradiation (min) for the 6 dosimeters used in this experiment.

Regarding the shelf life of the dosimeters, the refrigerated dosimeters responded to irradiation up to 11 days post-fabrication. Past this timeframe, oxygenation effects appeared in the dosimeter which resulted in areas of the dosimeter that did not respond to irradiation. The dosimeters stored at room temperature responded to irradiation up to 3 days post-fabrication. At 5 days post-fabrication, these dosimeters became unusable due to oxygen effects becoming visible (particularly polymerization of the gel, resulting in its contents pooling to the bottom of the PET jar) and the gel losing its viscosity. Hence, only two room temperature dosimeters were used in this experiment rather than the expected four.

4. Isocenter verification test

4.1 Overview

The isocenter verification test developed in this report is similar to the Winston Lutz test[16,18] in that it includes eight beams with geometries that span a range of couch and gantry angles. However, our method uses unique geometry for each beam such that they do not overlap anywhere except at the isocenter. These beams are delivered to a NIPAM dosimeter rather than the central BB used in the Winston Lutz test. The dosimeter is placed on the treatment table and aligned via the CBCT imaging system, irradiated, and a post-irradiation CBCT is acquired. Regions of the delivered dose are determined from the CBCT intensity values and the high dose area is analyzed to identify the beam trajectory relative to the imaging coordinate system. The steps of this comprehensive isocenter verification test are described in further detail in the sections below.

4.2 Materials and methods

4.2.1 Planning, irradiation, and imaging

The comprehensive isocenter verification test involves 8 radiation beams delivered to a NIPAM dosimeter at unique couch and gantry angles, as shown in Table 4. These beams are designed to be non-overlapping except at the isocenter. Although we used these specific beam trajectories in this report, the number of beams and their geometry does not necessarily need to be fixed to this specific geometry.

Table 4: Unique couch and gantry angles used in the comprehensive isocenter verification test.

Couch angle (°)	*Gantry angle (°)*
0	45
0	135
0	180
0	270
45	45
90	45
270	45
315	45

Figure 4 shows a 3D rendering of the dosimeter displaying the high dose volumes for the beam geometry.

Figure 4: 3D rendering of NIPAM dosimeter and high dose volume for the isocenter verification plan, obtained from Eclipse External Beam Planning.

The beam geometry in Table 4 was used to evaluate the radiation and imaging isocenters for a Varian STx linear accelerator with 6MV flattening filter free (FFF) photons and various collimation systems, including all SRS cone sizes (4 mm, 6 mm, 7.5 mm, 10 mm, 12.5 mm, and 15 mm diameter), as well as the high-definition multileaf collimator (HD-MLC) with a 5 mm field diameter. In each case, approximately 16 Gy was delivered per beam. We utilized Varian External Treatment Planning 15.6 (Varian Medical Systems, Inc) with the Anisotropic Analytical Algorithm (version 15.6.03) to calculate the dose for qualitative comparison and visualization of the dose distribution.

For each irradiation and imaging process, a NIPAM dosimeter was placed on the treatment table and centered using lasers and kV imaging, after which at least one CBCT image (pre-CBCT) was acquired. Then, without moving the dosimeter, the 8 beams from Table 4 were delivered, after which at least one CBCT image (post-CBCT) was again acquired. The CBCT settings varied depending on the experiment. The isocenter verification test performed using the MLCs, 4 mm cone, and 7.5 mm cone size used the following settings: full fan scan with bowtie filter, 80-120 kVp, 1035-4050 mAs, smooth reconstruction filter, and voxel dimensions of 0.5x0.5x1.0 mm^3. The test performed using the 6 mm, 10 mm, 12.5 mm, and 15 mm cone used the slow-mode CBCT scan. The CBCT settings using slow-mode were as follows: full fan scan with bowtie filter, 125 kVp, 5130 mAs, smooth reconstruction filter, and voxel dimensions of 0.5x0.5x1.0 mm^3. Between 1-3 pre- and post-CBCTs were acquired and averaged for the analysis.

4.2.2 Robustness and accuracy of the isocenter verification test

While performing the isocenter verification test, multiple pre- and post-CBCT images are acquired. This is done to average the images and test varying levels of image noise in the analysis. Hence, the analysis was carried out using 1, 2, or 3 averaged pre- and post-CBCTs. In addition to the automated analysis described in Section 4.2.2 and Appendix A, a manual analysis is also performed in which the central axis of each beam was determined via a manual registration and verification process. The resulting automatic and manual analysis results are then compared the results of a traditional Winston-Lutz test, film-based "star shots"[32], and the Varian Machine Performance Check (MPC). The 3D gantry isocenter diameter of the traditional Winston-Lutz test with MLCs was determined using the Pylinac package and compared with our results.

Because this isocenter verification test must be able to detect alignment errors, we created a test case to determine its ability of doing so. We applied a 0.5 mm shift to the MLCs along the direction of leaf travel (collimator at 45°) and repeated the isocenter verification test.

4.3 Analysis

The Matlab code used in this report to analyze the CBCT images has six primary steps: (1) detect the dosimeter in the CBCT, (2) remove the background, (3) define a region of interest (ROI) for each beam, (4) determine the beam geometry, (5) verify the

beam geometry, and (6) quantify relevant parameters. Each of these steps is described in further detail below.

4.3.1 Detecting the dosimeter

The first step involves detecting the dosimeter in the CBCT. It is identified in the post-CBCT and used as the region of interest (ROI) for the analysis. The ROI is defined using a voxel intensity threshold, and is further modified using a 3D erosion morphological operator[33] which removes all voxels within a certain number of voxels from the edges of the ROI. After erosion, the largest 3D object in the CBCT is selected as the final ROI.

4.3.2 Removing dosimeter background

Next, the background of the image is removed. The pre-CBCT is subtracted from the post-CBCT to help eliminate the background signal from the dosimeter and remove any artifacts from the reconstruction process. Because no shift was applied to the dosimeter during imaging and irradiation, any differences between the pre- and post-CBCTs should theoretically only be due to the chemical reactions of the gel dosimeter after irradiation.

4.3.3 Define an ROI for each beam

An ROI for each beam is defined to depict the individual trajectory of each beam through the dosimeter. Because the geometry of each beam is known (as demonstrated in Table 4), a 3D line for each beam is created to represent the predicted trajectory

through the dosimeter during irradiation. All voxels within a set distance (nominally 15 mm) of this 3D line are selected as an interim ROI. To avoid overlapping beams from interfering with the current ROI definition, the ROI is further confined to exclude any voxels that are in other beam paths. The final ROI is determined to be the intersection of the original interim ROI and the new, modified ROI.

4.3.4 Determine beam geometry

Once the ROIs have been determined for each beam, an iterative optimization using gradient descent is performed on the 3D lines of each beam to find the beam geometry that maximizes the CNR of the beam relative to the background of the dosimeter. At each iteration, the distance from the 3D line is calculated for all voxels within the defined ROI and the CNR is re-calculated.

4.3.5 Verify beam geometry

To verify the beam geometry as determined in the previous section, orthogonal 2D images are created through the CBCT for each beam, with the center of the beam shown as a 2D line. The resulting images are inspected visually to verify the beam geometry and ensuring that the 2D line is indeed along the center of the beam path.

4.3.6 Quantify relevant parameters

Once the trajectory of all eight beams have been determined, the code quantifies relevant parameters based on the actual beam geometry. These parameters include the minimum distance of each beam to the origin of the imaging coordinate system (imaging

isocenter), the smallest radius to encompass all beams, the location of the radiation isocenter relative to the imaging isocenter (the center of which is the radiation isocenter), and the actual couch and gantry angles. The couch angles are determined for all beams except those for which the geometry is parallel to the line defining the plane of the couch rotation (i.e. where the gantry is 0 degrees or 180 degrees).

4.4 Results

4.4.1 Radiation and imaging isocenter verification

Setup, irradiation, and imaging could be completed in under 38 minutes. An example of an irradiated dosimeter (using the 5 mm MLCs) is shown in Figure 5.

Figure 5: Irradiated dosimeter after performing the isocenter verification test using the 5 mm diameter MLCs.

Figure 6 shows the axial slice of the pre-irradiated CBCT (Figure 6a), post-irradiated CBCT (Figure 6b) and subtracted (Figure 6c) CBCT image (125 kVp, 1035 mAs, n=3) for the comprehensive isocenter verification test performed using the 5 mm

diameter MLC field. Figure 6 also shows the dosimeter after a applying a mask to the post-irradiated CBCT to eliminate the background (Figure 6d).

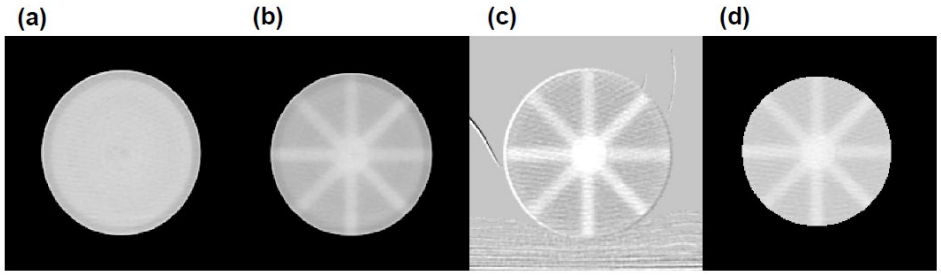

Figure 6: Axial slices of the (a) pre-CBCT image, (b) post-CBCT image, and (c) subtracted CBCT image for the isocenter verification test performed using the 5 mm diameter MLC field. Also shown in (d) is the dosimeter after applying a mask to eliminate the background.

After subtracting the background, the CNR of the high dose region increased from 3.9 to 5.4 with the test performed using the MLCs. A similar increased was observed for all SRS cones; for example, the CNR increased from 2.1 to 5.9 with the isocenter verification test performed using the 7.5 mm cone. Figure 7 shows the orthogonal slices of the processed CBCT for each beam; the beam center (as detected by the Matlab code) is also plotted for visual verification.

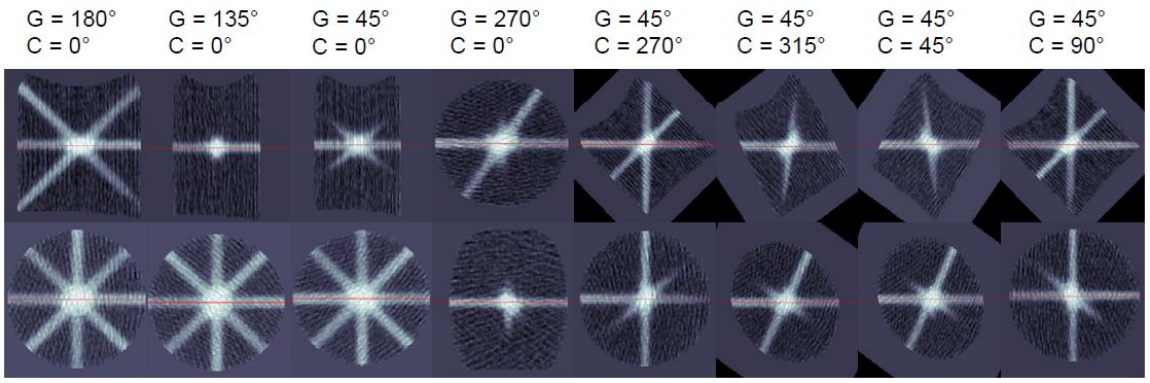

Figure 7: Orthogonal slices of the processed CBCT images of each beam using the 5 mm diameter MLC field. The gantry and couch angles are labeled above the corresponding orthogonal images.

Figure 8 shows orthogonal views through the dosimeter for the isocenter verification using the MLCs, 4 mm cone, and 7.5 mm cone. These three collimation systems are selected to demonstrate the differing beam diameters.

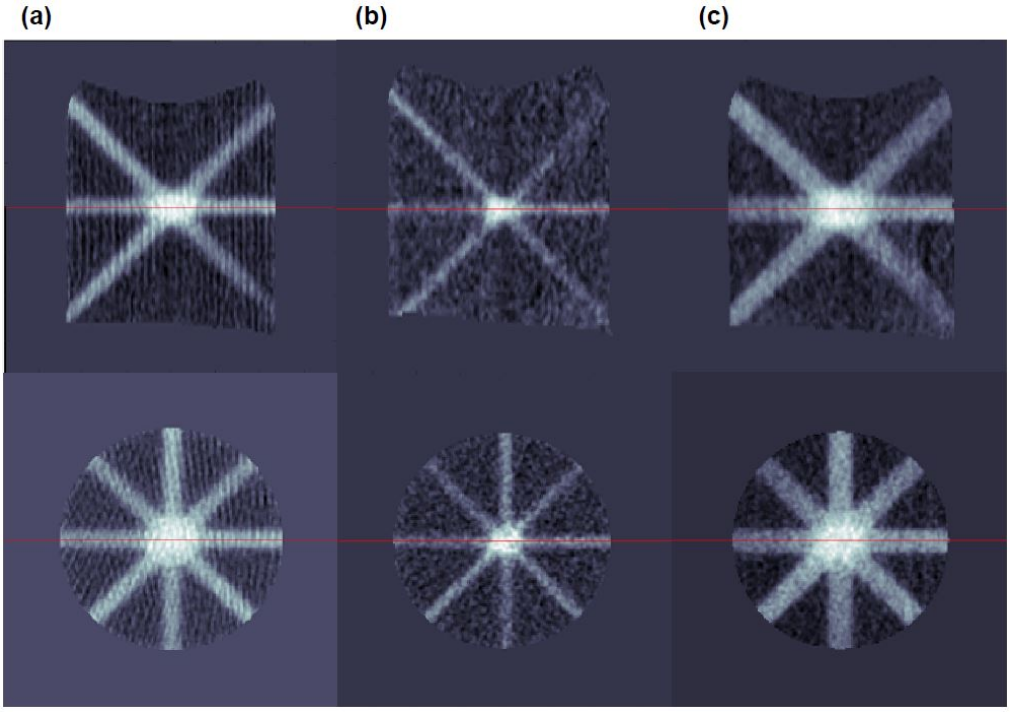

Figure 8: Orthogonal views through the dosimeter using the (a) 5 mm diameter MLC field, (b) 4 mm diameter cone, and (c) 7.5 mm diameter cone.

Table 5 shows the vector distance between radiation isocenter and CBCT origin, the smallest radius to encompass all radiation beams, and the difference between the measured and nominal gantry and couch angles as determined by the automatic analysis function of the Matlab code. Manual analysis of the MLCs and SRS cones showed improvement in the values listed in Table 5. The manual values are shown in Table 6.

Table 5: Automatic analysis results of the isocenter verification test using the MLCs and SRS cones.

	5 mm MLCs	*4 mm cone*	*6 mm cone*	*7.5 mm cone*	*10 mm cone*	*12.5 mm cone*	*15 mm cone*
Vector difference radiation isocenter to CBCT origin (mm)	0.39	0.21	0.23	0.45	0.15	0.65	0.14
Smallest radius that intersects all beams (mm)	0.38	0.44	0.53	0.48	0.75	0.5	0.57
Gantry accuracy mean differences (degrees)	0.16 ± 0.23	0.13 ± 0.16	0.38 ± 0.42	0.17 ± 0.23	0.56 ± 0.7	0.86 ± 0.74	0.47 ± 0.39
Couch accuracy mean difference (degrees)	-0.25 ± 0.27	0.04 ± 0.25	0.01 ± 0.45	0.16 ± 0.23	-0.08 ± 0.66	-0.29 ± 1.53	-0.07 ± 0.55

Table 6: Manual analysis results of the isocenter verification test using the MLCs and SRS cones.

	5 mm MLCs	*4 mm cone*	*6 mm cone*	*7.5 mm cone*	*10 mm cone*	*12.5 mm cone*	*15 mm cone*
Vector difference radiation isocenter to CBCT origin (mm)	0.19	0.14	0.14	0.10	0.11	0.18	0.08
Smallest radius that intersects all beams (mm)	0.28	0.40	0.33	0.41	0.61	0.48	0.34
Gantry accuracy mean differences (degrees)	0.03 ± 0.08	-0.07 ± 0.37	0.11 ± 0.06	0.05 ± 0.08	0.09 ± 0.18	0.03 ± 0.06	0.04 ± 0.07
Couch accuracy mean difference (degrees)	-0.01 ± 0.22	0.04 ± 0.07	-0.01 ± 0.18	-0.08 ± 0.14	0.44 ± 0.49	-0.03 ± 0.4	-0.07 ± 0.11

To determine the reproducibility of the comprehensive isocenter verification test, we repeated the test using the 6 mm cone. As shown in Table 5, the automatic analysis determined the vector difference between the radiation and CBCT origin and smallest radius to intersect all radiation beams to be 0.23 mm and 0.53 mm, respectively. When the test was repeated, these values were found to be 0.24 mm and 0.53 mm, respectively.

4.4.2 Robustness and accuracy of the isocenter verification test

In comparison to Tables 5 and 6, traditional star shots for the couch and gantry indicated a minimum tangent circle radius for the same linear accelerator of 0.18 mm and 0.28 mm, respectively. As a second comparison, the Pylinac package was used to evaluate traditional Winston-Lutz images with MLCs and indicated a 3D isocenter radius of 0.24 mm. This matched the isocenter size measured by the Varian MPC. The Varian MPC also measured the kV imager projection offset to be +0.25 mm.

4.4.3 Detecting alignment error

The automatic isocenter analysis was able to detect the change in radiation isocenter size when the 0.5 mm shift was applied to the MLC isocenter verification plan. With the shift applied to each MLC field, the vector difference between the radiation isocenter and CBCT origin increased from 0.4 mm to 0.6 mm, and the radiation isocenter radius increased from 0.4 mm to 0.9 mm. Figure 9 shows the 3D plots showing the

displacement of the beams with the 0.5 mm shift compared to the 5 mm MLC field test and an ideal isocenter verification test.

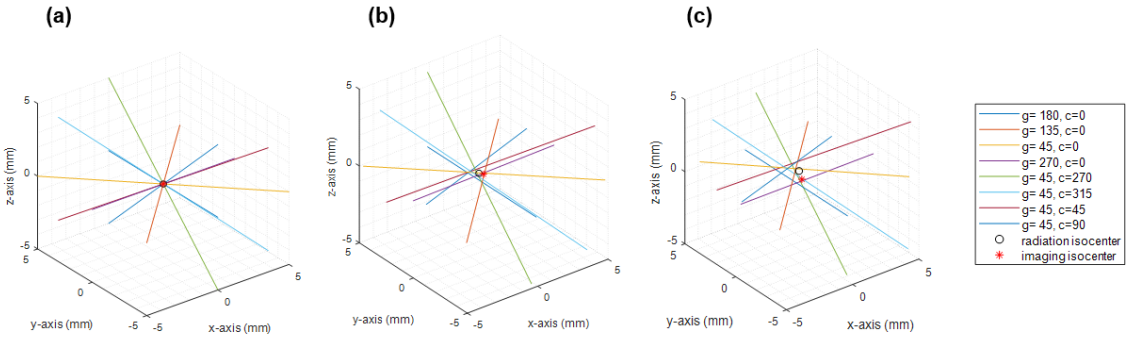

Figure 9: 3D plot of each beam's central axis for (a) ideal case with no uncertainty in radiation and imaging isocenter alignment, (b) measured beam trajectories for the 5 mm diameter MLC field, and (c) measured beam trajectories with the 0.5 mm error applied.

4.4.4 Relationship between CNR and accuracy of isocenter verification test

The experimental measurements performed were designed to maximize the CNR of the dose signal in the CBCT image for the isocenter verification test. Here we report the relationship between CNR and the accuracy of the test to assess the value in performing these steps to try increasing CNR. Looking specifically at the tests performed using the MLCs and 7.5 mm cone, when three pre- and post-irradiation CBCTs were averaged, the CNR was 4.9 and 5.9, respectively. In comparison, when only one CBCT image was used (no averaging performed) the CNR decreased to 3.1 and 3.2 for the MLCs and 7.5 mm cone. This decrease in CNR has relatively little effect on the isocenter analysis, however. When only one CBCT was used the mean absolute difference in the detected distance from the radiation isocenter and CBCT origin was

0.03 mm n each axis for the MLCs and 0.03 mm, 0.01 mm, and 0.06 mm in x, y, and z axes for the 7.5 mm cone. The mean absolute difference per beam was 0.01±0.02 mm and 0.01±0.04 mm for the MLCs and 7.5 mm cone, respectively. Figure 10 shows three separate plots as a function of CNR for each beam: the difference between automatic and manual analysis for the radiation isocenter size (Figure 10a), the difference between measured and nominal gantry angles (Figure 10b), and the difference between measured and nominal couch angles (Figure 10c). The R-squared value for these plots are 0.0017, 0.1326, and 0.0103, respectively. This does not indicate a strong relationship between CNR and experimental measurements.

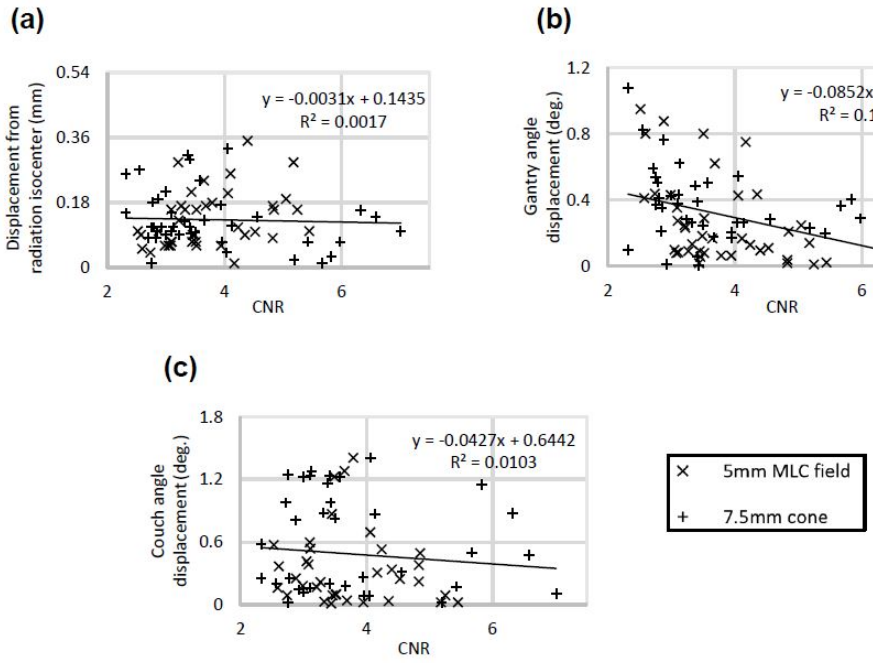

Figure 10: Scatter plots of the relationship between CNR and various parameters: (a) the absolute displacement from the measured and nominal distance between the radiation isocenter, (b) gantry angles, and (c) couch angles of the 5 mm diameter MLCs and 7.5 mm cone.

4.5 Discussion

We have successfully demonstrated a comprehensive method to visualize and quantify the uncertainty in the radiation isocenter and coincidence with the kV-CBCT imaging coordinate system using 3D NIPAM gel dosimeters. The primary advantage of using kV-CBCT dosimetry is that the dose information is read out in the same coordinate system as radiation delivery so there is no need for an independent readout system (such as optical CT or a flatbed scanner), and no need to send off for outside analysis. Image fusion/registration is also not necessary as the dose is already incorporated into the CBCT image and treatment planning system for analysis. The comprehensive isocenter verification test was shown to be applicable to MLCs and cones, and in theory could be applied to other collimation system as well as off-axis and multiple-target geometries.

Another advantage of the comprehensive isocenter verification test is that it is not affected by the initial setup of the gel dosimeter, which helps to eliminate potential false positives based on initial setup errors. Traditional isocenter verification methods, such as the Winston-Lutz test, utilize a phantom or apparatus aligned with lasers to the isocenter; any misalignment of the phantom may be propagated into the results of the isocenter verification test results. These setup errors can be on the same order of magnitude as those being measured, and thus may lead to false positives of the test (i.e. the measurements show that there is misalignment when there is not). In comparison,

the technique presented in this report is largely insensitive to the setup and alignment of the dosimeter provided that the radiation beams and isocenter fall within the gel dosimeter. Lastly, traditional isocenter verification tests quantify uncertainties in radiation and imaging coordinate systems separately. This makes it more difficult to fully assess the interaction between uncertainties between the two systems. The NIPAM kV-CBCT technique uses the trajectories of each radiation beam which are individually measured directly in the imaging coordinate system.

Our measured values of the minimum radius of the radiation isocenter (0.52 mm on average for the seven collimation systems used in this report) were slightly higher than the values the traditional Winston-Lutz test and Varian MPC test produced (0.24 mm for both tests). One possible explanation for this increase is noise or uncertainty in the detection accuracy of the CBCT. For example, the voxel size in the axial dimension is 1 mm which may limit the detectable resolution of the comprehensive isocenter test. However, sub-mm detection accuracy is still achievable (as shown in Figure 9) since all the voxels in the beam path can be incorporated and for any given beam the distance of each voxel from the central axis is determined by exact geometry. A second possible explanation for the slight difference in radiation radius could be movement of the dosimeter or couch sag during the irradiation and imaging process. We suspect this as the most plausible case for two reasons: (1) the dosimeter was fixed to the treatment table with tape rather than a more sophisticated immobilization method, and (2) the

edge of the detector did not cancel out completely when the pre-CBCT was subtracted from the post-CBCT (as shown in Figure 6c). To verify this was the case, we registered the pre-CBCT with the post-CBCT and quantified the translation of the dosimeter using the 5 mm diameter MLCs, 4 mm cone, and 7.5 mm cone. After registration, we found a translation of [0.0 mm, 0.0 mm, 0.1 mm], [0.0 mm, 0.1 mm, 0.0 mm] , and [0.0 mm, 0.0 mm, 0.0 mm] in the [X, Y, Z] dimensions for the 5 mm MLC field, 4 mm cone, and 7.5 mm cone, respectively. These differences are small from a clinical perspective but may be large enough to explain the differences between our radiation isocenter radius results and those of the traditional Winston-Lutz test and Varian MPC test.

We used CNR to quantify the detectability of the dose profile in the CBCT image for this study. This was by no means the only way to perform this analysis; our justification for using a CNR-based approach is that a higher CNR value corresponds to greater spatial accuracy of an image, although the CNR values in this report are relatively low. However, because we are detecting a beam location, we aren't necessarily interested in the absolute accuracy of the voxel intensity. This comprehensive isocenter verification test is not nearly as sensitive to CNR as other potential approaches, which also means it is not as sensitive to changes in intensity over time. Nevertheless, various methods were used in this report to increase the CNR, such as averaging CBCT images, applying a smooth reconstruction filter, waiting to acquire post-CBCT images to allow chemical reactions within the gel to stabilize and increase dose sensitivity, and using a

slow-mode CBCT scan on several tests to increase the number of projections. Applying these methods do increase the CNR, but they are not essential to the comprehensive isocenter verification test, as demonstrated in Figure 10.

While we present the use of kV-CBCT dosimetry to radiosurgery, other 3D dosimetry system have been applied as well[29,34,35]. These systems often rely on magnetic resonance imaging (MRI) or optical CT to read out the change in optical density within the dosimeters after irradiation. These systems are not always readily available, whereas CBCT is and will be in the same frame of reference as the radiation delivered. Another major difference between our work and prior work is that our test uses a specific geometry to verify the radiation and imaging isocenters rather than using 3D dosimetry to verify the accuracy of a specific dose distribution.

One question that arises is what the optimal use would be of this comprehensive isocenter verification test. The test has potential for use with linear accelerator acceptance and commissioning, verification after machine maintenance or repairs, and routine QA. Because isocenter verification is performed daily prior to treatment for SRS linear accelerators, the optimal use for this comprehensive isocenter test would most likely be for less frequent QA (such as annual, quarterly, or monthly), provided the Winston-Lutz test be performed daily using the portal imager. The question of whether the cost of the dosimeter would be prohibitive for more frequent QA is the primary reason for suggesting the optimal use be for less frequent QA. Given our material costs,

we estimate the cost of one 16 oz. dosimeter to be roughly $40, which is likely a feasible amount for less frequent routine QA. Although in this report we prepared the dosimeters in-house, an expected prerequisite for routine clinical use would be to purchase the dosimeters from an existing vendor. If the dosimeters were purchased externally rather than fabricated in-house, then the expected time required to complete QA would be similar to that of the traditional Winston-Lutz test; the setup time would be slightly less (since the technique is not as sensitive to manual setup), while the imaging and irradiation time would be slightly more (requires 2 CBCTs and delivery of 16 Gy per beam).

There are several limitations to the current study. The Matlab code used to analyze the CBCTs used a CNR-based method to determine the beam incidence. Other, more robust, methods could have been applied that improve detection accuracy. Second, accuracy of the detected radiation isocenter as well as the couch and gantry angles are dependent on the size of the dosimeter jar. We use a single dosimeter size (16 oz.) throughout this study to demonstrate feasibility; future work will include using larger dosimeter sizes to investigate the required size necessary to achieve a given level of detection accuracy.

5. Conclusion

We have demonstrated the ability of using a 3D NIPAM gel dosimeter for comprehensive verification of the radiation isocenter uncertainty, coincidence with the kV-CBCT imaging system, as well as couch and gantry angle accuracy. This technique can be carried out in under 40 minutes, making it an ideal candidate for QA purposes. It is applicable to any collimation system (MLCs or cone) and can detect and visualize sub-mm alignment errors in the collimation system.

References

1. Siegel RL, Miller KD, Jemal A. Cancer statistics, 2015. *CA Cancer J Clin*. 2015;65(1):5-29. doi:10.3322/caac.21254

2. Nagata Y. Stereotactic body radiotherapy for early stage lung cancer. *Cancer Res Treat*. 2013;45(3):155-161. doi:10.4143/crt.2013.45.3.155

3. Folkert MR, Bilsky MH, Tom AK, et al. Outcomes and toxicity for hypofractionated and single-fraction image-guided stereotactic radiosurgery for sarcomas metastasizing to the spine. *Int J Radiat Oncol Biol Phys*. 2014;88(5):1085-1091. doi:10.1016/j.ijrobp.2013.12.042

4. Kim YJ, Cho KH, Kim JY, et al. Single-dose versus fractionated stereotactic radiotherapy for brain metastases. *Int J Radiat Oncol Biol Phys*. 2011;81(2):483-489. doi:10.1016/j.ijrobp.2010.05.033

5. Jaffray DA, Siewerdsen JH, Wong JW, Martinez AA. Flat-panel cone-beam computed tomography for image-guided radiation therapy. *Int J Radiat Oncol Biol Phys*. 2002;53(5):1337-1349. http://www.ncbi.nlm.nih.gov/pubmed/12128137.

6. Smitsmans MHP, de Bois J, Sonke J-J, et al. Automatic prostate localization on cone-beam {CT} scans for high precision image-guided radiotherapy. *Int J Radiat Oncol*. 2005;63(4):975-984. doi:10.1016/j.ijrobp.2005.07.973

7. Adamson J, Wu Q. Inferences About Prostate Intrafraction Motion From Pre- and Posttreatment Volumetric Imaging. *Int J Radiat Oncol*. 2009;75(1):260-267. doi:10.1016/j.ijrobp.2009.03.007

8. Bissonnette J-P, Purdie TG, Higgins JA, Li W, Bezjak A. Cone-Beam Computed Tomographic Image Guidance for Lung Cancer Radiation Therapy. *Int J Radiat Oncol*. 2009;73(3):927-934. doi:10.1016/j.ijrobp.2008.08.059

9. Tree AC, Alexander EJ, Van As NJ, Dearnaley DP, Khoo V. Biological Dose Escalation and Hypofractionation: What is There to be Gained and How Will it Best be Done? *Clin Oncol*. 2013;25(8):483-498. doi:10.1016/j.clon.2013.05.003

10. Dai J, Zhu Y, Qu H, et al. A method for repositioning of stereotactic brain patients

with the aid of real-time CT image guidance. *Phys Med Biol Phys Med Biol*. 2005;50:201-207. doi:10.1088/0031-9155/50/16/N01

11. Dhabaan A, Schreibmann E, Siddiqi A, et al. Six degrees of freedom CBCT-based positioning for intracranial targets treated with frameless stereotactic radiosurgery. *J Appl Clin Med Phys*. 2012;13(6):215-225. doi:10.1120/jacmp.v13i6.3916

12. Solberg TD, Balter JM, Benedict SH, et al. Quality and safety considerations in stereotactic radiosurgery and stereotactic body radiation therapy: Executive summary. *Pract Radiat Oncol*. 2012;2(1):2-9. doi:10.1016/J.PRRO.2011.06.014

13. Klein EE, Hanley J, Bayouth J, et al. Task Group 142 report: Quality assurance of medical acceleratorsa). *Med Phys*. 2009;36(9Part1):4197-4212. doi:10.1118/1.3190392

14. Faught AM, Trager M, Yin F-F, Kirkpatrick J, Adamson J. Re-examining TG-142 recommendations in light of modern techniques for linear accelerator based radiosurgery. *Med Phys*. 2016;43(10):5437-5441. doi:10.1118/1.4962471

15. González A, Castro I, Martínez JA. A procedure to determine the radiation isocenter size in a linear accelerator. *Med Phys*. 2004;31(6):1489-1493. doi:10.1118/1.1755491

16. Lutz W, Winston KR, Maleki N. A system for stereotactic radiosurgery with a linear accelerator. *Int J Radiat Oncol Biol Phys*. 1988;14(2):373-381. http://www.ncbi.nlm.nih.gov/pubmed/3276655. Accessed June 27, 2019.

17. Clivio A, Vanetti E, Rose S, et al. Evaluation of the Machine Performance Check application for TrueBeam Linac. *Radiat Oncol*. 2015;10(1):97. doi:10.1186/s13014-015-0381-0

18. Gao J, Liu X, Gao J, Liu X. Off-Isocenter Winston-Lutz Test for Stereotactic Radiosurgery/Stereotactic Body Radiotherapy. *Int J Med Physics, Clin Eng Radiat Oncol*. 2016;05(02):154-161. doi:10.4236/ijmpcero.2016.52017

19. Schreiner LJ. True 3D chemical dosimetry (gels, plastics): Development and clinical role Related content Radiochromic 3D Detectors Mark Oldham-Audits for advanced treatment dosimetry G S Ibbott and D I Thwaites-Programme-Recent

citations True 3D chemical dosimetry (gels, plastics): Development and clinical role. *J Phys Conf Ser OPEN ACCESS*. doi:10.1088/1742-6596/573/1/012003

20. Hashemi B, Zahmatkesh MH. A new approach to radiochromic three-dimensional dosimetry-polyurethane. *J Phys Conf Ser OPEN ACCESS*. 2004. doi:10.1088/1742-6596/3/1/020

21. Venning AJ, Hill B, Brindha S, Healy BJ, Baldock C. Investigation of the PAGAT polymer gel dosimeter using magnetic resonance imaging. *Phys Med Biol*. 2005;50(16):3875-3888. doi:10.1088/0031-9155/50/16/015

22. Hsieh BT, Chang YJ, Han RP, Wu J, Hsieh LL, Chang CJ. A study on dose response of NIPAM-based dosimeter used in radiotherapy. In: *Journal of Radioanalytical and Nuclear Chemistry*. Vol 290. ; 2011:141-148. doi:10.1007/s10967-011-1161-4

23. Sakhalkar HS, Adamovics J, Ibbott G, Oldham M. A comprehensive evaluation of the PRESAGE/optical-CT 3D dosimetry system. *Med Phys*. 2009;36(1):71-82. doi:10.1118/1.3005609

24. McJury M, Oldham M, Cosgrove VP, et al. Radiation dosimetry using polymer gels: Methods and applications. *Br J Radiol*. 2000;73(873):919-929. doi:10.1259/bjr.73.873.11064643

25. Baldock C, De Deene Y, Doran S, et al. Polymer gel dosimetry. *Phys Med Biol*. 2010;55(5):R1--R63. doi:10.1088/0031-9155/55/5/R01

26. Maynard E, Hilts M, Heath E, Jirasek A. Evaluation of accuracy and precision in polymer gel dosimetry. *Med Phys*. 2017;44(2):736-746. doi:10.1002/mp.12080

27. Day MJ, Stein G. Chemical effects of ionizing radiation in some gels. *Nature*. 1950;166(4212):146-147. doi:10.1038/166146a0

28. Senden RJ, De Jean P, Mcauley KB, Schreiner LJ. Polymer gel dosimeters with reduced toxicity: a preliminary investigation of the NMR and optical dose-response using different monomers. *Phys Med Biol*. 2006;51:3301-3314. doi:10.1088/0031-9155/51/14/001

29. Adamson J, Carroll J, Trager M, et al. Delivered Dose Distribution Visualized Directly With Onboard kV-CBCT: Proof of Principle. *Int J Radiat Oncol*. 2019;103(5):1271-1279. doi:10.1016/j.ijrobp.2018.12.023

30. *Catphan 504 Manual*.; 2013. https://static1.squarespace.com/static/5367b059e4b05a1adcd295c2/t/551ae42be4b046662454b34d/1427825707349/catphan504manual.pdf. Accessed August 22, 2019.

31. Maynard E, Hilts M, Heath E, Jirasek A. Evaluation of accuracy and precision in polymer gel dosimetry. *Med Phys*. 2017;44(2):736-746. doi:10.1002/mp.12080

32. Depuydt T, Penne R, Verellen D, et al. Computer-aided analysis of star shot films for high-accuracy radiation therapy treatment units. *Phys Med Biol*. 2012;57(10):2997-3011. doi:10.1088/0031-9155/57/10/2997

33. Heijmans H. *Morphological Image Operators*. Vol 4. Boston MA: Academic Press, Inc.; 1994.

34. Novotný J, Dvořák P, Spěváček V, et al. Quality control of the stereotactic radiosurgery procedure with the polymer-gel dosimetry. *Radiother Oncol*. 2002;63(2):223-230. doi:10.1016/S0167-8140(02)00064-6

35. Thomas A, Niebanck M, Juang T, Wang Z, Oldham M. A comprehensive investigation of the accuracy and reproducibility of a multitarget single isocenter VMAT radiosurgery technique. *Med Phys*. 2013;40(12):121725. doi:10.1118/1.4829518